Electronic conductivity in Ni_xCr_{1-x} and Ni_xCu_{1-x} fcc alloy systems

A. Vernes

Center for Computational Materials Science, Technical University Vienna, Gumpendorferstrasse 1a, A−1060 Vienna, Austria

H. Ebert

Institut für Physikalische Chemie, Universität München, Butenandtstrasse 5−13, D−83177 München, Germany

J. Banhart

Hahn-Meitner-Institut, Glienicker Strasse 100, D−14109 Berlin, Germany

First-principles calculations of transport properties of disordered alloys based on the Kubo-Greenwood formalism and the spin-polarized Korringa-Kohn-Rostoker coherent potential approximation are presented. Application to the fcc alloy systems Ni_xCr_{1-x} and Ni_xCu_{1-x} yields results for the residual resistivity, anomalous magnetoresistance, and the magnetic moments that are in very satisfying agreement with experiment. In particular, the different sign for the resistance anisotropy in Ni_xCr_{1-x} and Ni_xCu_{1-x} and the concentration of the onset of magnetism could be reproduced. Scalar-relativistic calculations were performed on the basis of the two-current model in order to assess the importance of relativistic effects in these systems.

I. INTRODUCTION

Galvanomagnetic effects in ferromagnetic alloy systems, such as the anomalous magnetoresistance (AMR) (sometimes called spontaneous magnetoresistance anisotropy) and the anomalous Hall resistivity (AHR) have been used for many years in the sensor technology.[1] The discovery of the so-called giant magnetoresistance (GMR) in multilayer systems[2] and recently of the colossal magnetoresistance (CMR) in perovskites[3] with promising technological prospects also renewed interest in the conventional galvanomagnetic or magnetoresistance phenomena. Although it has been known for more than 40 years that these phenomena have an intrinsic origin, namely, the interplay of the spin-orbit coupling (SOC) and spontaneous magnetization,[4] a realistic theoretical description accounting for both sources could be given only recently.[5]

This theoretical approach combines the Kubo-Greenwood formalism[6,7] with a fully relativistic description of the underlying electronic structure. It has been successfully applied in detailed investigations of the residual resistivity and AMR in several random alloy systems.[8–12] Application of a spin-polarized relativistic scheme is necessary to account for the symmetry reduction caused by the simultaneous presence of SOC and spontaneous magnetization in a parameter-free way. Solving the Dirac equation within the Korringa-Kohn-Rostoker (KKR) coherent potential approximation (CPA), the Kubo-Greenwood equation can be used straightforwardly to calculate the residual resistivity tensor elements. Furthermore, by manipulating the SOC,[13,14] one gets access—in contrast to the familiar two-current model[15] used in the past—to the spin-dependent scattering mechanisms, which are sources for the AMR, in a first-principles manner.[8,12]

The fcc alloy systems Ni_xCr_{1-x} and Ni_xCu_{1-x} were chosen for the present study because of their interesting transport and magnetic properties and also because of the availability of experimental data. Both alloy systems exist in a paramagnetic and ferromagnetic state with a phase transition at a critical Ni concentration (depending on the alloy system) without changing their crystal structure.[16,17] This permits in principle to apply the adopted theoretical description to the para- as well as ferromagnetic phases. However, a direct comparison with experiment is problematic for the paramagnetic phase close to the phase transition, because of the occurrence of giant magnetic moments.[16,18] Furthermore, an anomalous temperature dependence of the resistivity near the critical composition is also characteristic for both alloys.[19–21] In addition, for Ni_xCu_{1-x} the magnetic phase transition is preceded by a superparamagnetic state[22] followed by a spin-glass-like ordering.[23,24] The Ni_xCr_{1-x} alloy system is known to possess so-called virtual bound states (VBS) in their density of states,[15] giving rise to further peculiarities, such as a negative AMR ratio[25] and average alloy moments that do not follow the general trend of a Slater-Pauling plot.[26] For these reasons we present not only theoretical results on the galvanomagnetic properties of Ni_xCr_{1-x} and Ni_xCu_{1-x}, but also data connected to their electronic and magnetic properties obtained within fully and scalar-relativistic calculations.

II. THEORETICAL FRAMEWORK

For ferromagnetic cubic solids with magnetization along the z axis, the resistivity tensor

$$\boldsymbol{\rho} = \boldsymbol{\sigma}^{-1} = \begin{pmatrix} \rho_\perp & -\rho_H & 0 \\ \rho_H & \rho_\perp & 0 \\ 0 & 0 & \rho_\parallel \end{pmatrix} \qquad (1)$$

reflects the reduced symmetry of the system. In the paramagnetic case this tensor is diagonal with all elements identical. The tensor elements $\rho_\perp$ and $\rho_\parallel$ are the transverse (for current perpendicular to the magnetization) and longitudinal (for current parallel to the magnetization) resistivities, while ρ_H denotes the spontaneous or anomalous Hall resistivity. The anomalous magnetoresistance ratio is defined by

$$\frac{\Delta\rho}{\bar{\rho}} = \frac{\rho_{\parallel} - \rho_{\perp}}{\bar{\rho}}. \tag{2}$$

Here $\bar{\rho}$ is the isotropic resistivity that is obtained by averaging the diagonal elements of the resistivity tensor (1), i.e.,

$$\bar{\rho} = \frac{1}{3}(2\rho_{\perp} + \rho_{\parallel}). \tag{3}$$

Most ferromagnetic alloy systems show a positive AMR ratio, i.e., $\rho_{\parallel} > \rho_{\perp}$. However, in systems such as Ni_xCr_{1-x}, the opposite situation ($\rho_{\parallel} < \rho_{\perp}$) appears. Experimentally, the AMR ratio and $\bar{\rho}$ are obtained by measuring the longitudinal and transverse resistivity as a function of the applied external magnetic field and then extrapolating the results to zero field.

An efficient method for calculating the diagonal elements of the resistivity tensor (1) for disordered alloys is given by linear response theory via the Kubo-Greenwood equation[6,7]

$$\rho_{\mu\mu}^{-1} = \frac{\hbar}{\pi V_{cryst}} \text{Tr}\langle j_{\mu} \text{Im}\, G^+(E_F) j_{\mu} \text{Im}\, G^+(E_F) \rangle_{conf}. \tag{4}$$

Here j_{μ} is the μ spatial component of the electronic current density operator $\mathbf{j}$ and $G^+(E_F)$ the positive side limit of the single-particle Green function at the Fermi energy E_F. Using multiple scattering theory in combination with the Korringa-Kohn-Rostoker (KKR) method of band structure calculation, the electronic Green function in real space can be determined with a very high accuracy expressed in terms of the so-called scattering-path operator τ (Ref. 27)

$$G^+(\mathbf{r}_n, \mathbf{r}_m, E) = \sum_{QQ'} Z_Q^n(\mathbf{r}_n, E) \tau_{QQ'}^{nm}(E) Z_{Q'}^{m\times}(\mathbf{r}_m, E)$$
$$+ G_{irr}^+(\mathbf{r}_n, \mathbf{r}_m, E), \tag{5}$$

where $Z_Q^n(\mathbf{r}_n, E)$ are the regular solutions of the Schrödinger (or Dirac) equation for the potential well at lattice site n. The part involving the irregular solutions, $G_{irr}^+(\mathbf{r}_n, \mathbf{r}_m, E)$, can be suppressed in Eq. (4) because it is purely real within the atomic sphere approximation. The combined quantum number index Q stands in the nonrelativistic or scalar-relativistic case for (l, m_l) and the relativistic case for $\Lambda \equiv (\kappa, \mu)$.[28]

Using the Green function obtained by applying the coherent potential approximation (KKR-CPA), Eq. (4) provides the residual resistivity for randomly disordered alloy systems at $T = 0$ K. This implies that for the resistivity only the chemical disorder is accounted for, while other contributions coming from lattice imperfections, grain boundaries, phonons, magnons are neglected. Accordingly, the average $\langle \cdots \rangle_{conf}$ in Eq. (4) stands for the configurational average of a disordered alloy. The way in which this configurational average of two Green functions can be evaluated within the KKR-CPA was first worked out by Butler.[29] Since then the scheme has been applied with success to a variety of paramagnetic alloy systems.[8–12,30]

Recently, it has become possible to extend Butler's formulas to deal with ferromagnetic alloy systems[5] within the spin polarized relativistic (SPR) version of the KKR-CPA.[31]

This was a necessary step to be made, because only the fully relativistic description of the underlying electronic structure of ferromagnets accounts properly for the reduced symmetry induced by the simultaneous occurrence of the spontaneous magnetization and spin-orbit coupling. Our SPR-KKR-CPA version of the Kubo-Greenwood formalism includes all relativistic effects, in particular, the so-called scalar-relativistic effects, namely the Darwin and the mass-velocity term and the spin-orbit coupling. For a detailed study of the impact of these relativistic effects on the galvanomagnetic properties of ferromagnetic alloy systems, see Ref. 8.

Often galvanomagnetic properties are discussed on the basis of the two-current model (see, for example, Ref. 10 and the references therein). This model accounts for the two sources of the AMR, the spin polarization and spin-orbit coupling, in a rather simple manner assuming the relation

$$\frac{\Delta\rho}{\bar{\rho}} = \gamma\left(\frac{\rho^{\downarrow}}{\rho^{\uparrow}} - 1\right). \tag{6}$$

Here γ is a measure for the strength of the spin-orbit coupling. The subband resistivities $\rho^{\uparrow}$ and $\rho^{\downarrow}$ are assumed to contribute independently to the total resistivity, like two parallel resistors do, leading to the averaged resistivity

$$\frac{1}{\bar{\rho}} = \frac{1}{\rho^{\downarrow}} + \frac{1}{\rho^{\uparrow}}. \tag{7}$$

Neither $\rho^{\downarrow}$, $\rho^{\uparrow}$ nor γ can be measured directly. The former are usually determined from deviations from Matthiesen's rule for ternary alloys or from the temperature dependence of the resistivity of binary alloys.[32] In contrast to this, within a scalar-relativistic calculation, where the spin-orbit coupling is not taken into account, one has direct access to the two subband resistivities $\rho^{\downarrow}$ and $\rho^{\uparrow}$. The parameter γ can be deduced from experimental data on the basis of Eq. (6) assuming that it is concentration independent.[10,33] Hence, the experimental data for γ cannot prove the applicability of the two-current model, because its validity is implicitly accepted when γ is calculated from Eq. (6).

Our previous work has shown that the simple two-current model works well for systems without high spin polarization, such as fcc Co_xPd_{1-x} or fcc Co_xPt_{1-x},[9] but fails for Ni-based binary alloy systems, such as fcc Fe_xNi_{1-x} and fcc Co_xNi_{1-x}, for which a high spin polarization at the Fermi level occurs.[10] In the latter case even an extended two-current model including the rate of spin-flip transitions does not lead to significant improvements compared to fully relativistic results. Furthermore, it was shown in Refs. 9 and 10 that γ has a rather pronounced dependence on the concentration. Therefore, in the present paper we compared the fully relativistically calculated AMR ratio only with the scalar-relativistically obtained $\rho^{\downarrow}/\rho^{\uparrow} - 1$ term [see Eq. (6)]. In spite of the questionable applicability of the two-current model, it appears to remain a very simple tool to interpret and understand the galvanomagnetic properties of ferromagnetic alloy systems on an intuitive basis. For that reason we have used it in the following.
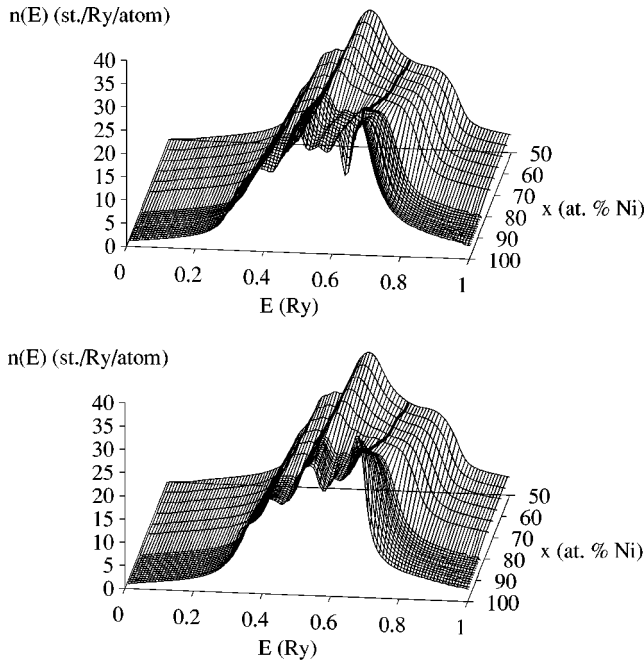
FIG. 1. Spin-projected density of states $n(E)$ as a function of Ni content for Ni$_x$Cr$_{1-x}$ ($50\% \leqslant x_{\text{Ni}} \geqslant 95\%$) obtained using the SPR-KKR-CPA method. Projection of the density of states into majority and minority spin subsystem is given in the top and bottom panel, respectively. The bold solid line represents the Fermi level.

All the results presented in this paper were obtained using either the relativistic or the scalar-relativistic version of the Kubo-Greenwood formalism including CPA-vertex corrections. Matrix elements up to $l_{\text{max}} = 3$ were considered in all of the calculations.

III. RESULTS AND DISCUSSION

A. Electronic properties

The fully relativistic density of states as a function of Ni concentration projected into the majority and minority spin channel is given in Figs. 1 and 2 for Ni$_x$Cr$_{1-x}$ and Ni$_x$Cu$_{1-x}$, respectively. Comparing these two figures, one observes that the changes in the density of states upon addition of Cr or Cu to Ni are quite different. This well-known scattering center effect[25] shows up already for small concentrations of the impurity and its manifestation depends on the character of the impurity potential relative to the host (in this case Ni). The less attractive potential of Cr induces resonant d states in the vicinity of the Fermi level, the so-called virtual bound states (VBS's),[34] which do not appear in Ni$_x$Cu$_{1-x}$ due to the more attractive potential of Cu. For this reason, in the latter case the states near the Fermi level are almost entirely dominated by the Ni d states.

In the past it was often assumed that VBS's appear only in the spin-up subsystem.[35] However, calculations using the KKR Green function method[36] have shown that the virtual bound states induced by Cr impurity in Ni exist in both spin channels. Our SPR-KKR-CPA calculations (shown in Fig. 1) complete this by demonstrating that the virtual bound states induced by Cr persist over a wide concentration range and dominate the entire ferromagnetic phase of Ni$_x$Cr$_{1-x}$ for
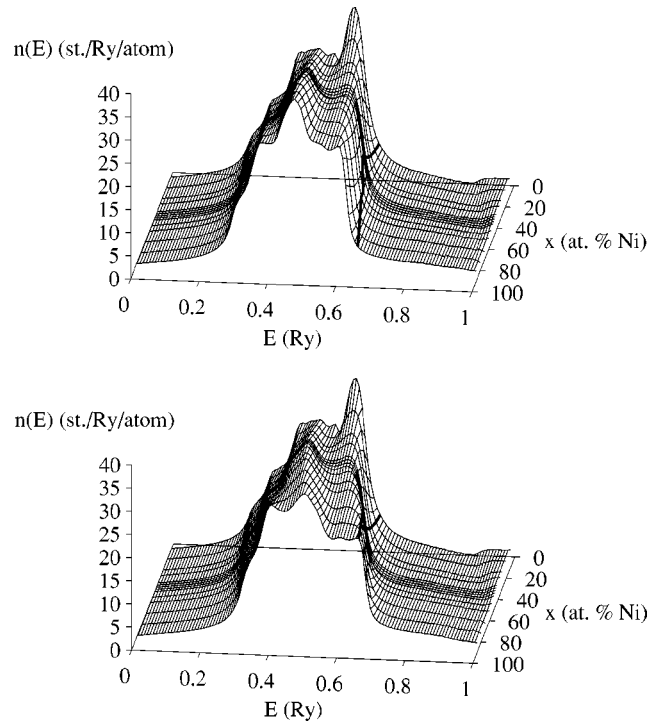
FIG. 2. As in Fig. 1, but for Ni$_x$Cu$_{1-x}$ ($0 \leqslant x_{\text{Ni}} \leqslant 80\%$).

both spin directions. Furthermore, the density of states at the Fermi level in the majority subsystem is always higher than that in the minority subsystem. Connected with this, it was found that the local magnetic moment of Cr is always antiparallel to that of Ni (see Sec. III B). As a consequence, the minority subband resistivity is smaller than that for the majority subsystem. This gives a simple explanation for the observed negative AMR (a more detailed discussion will be given in Sec. III C 2) derived within the two-current model. Apparently, the peak in the density of states curve of Ni$_x$Cr$_{1-x}$ identified as a VBS disappears if the Cr content further increases. However, the partial density of states of Cr (not given in Fig. 1) shows that the partially filled peak originating from Cr persists throughout the entire concentration range.

In contrast to Ni$_x$Cr$_{1-x}$, the density of states for ferromagnetic Ni$_x$Cu$_{1-x}$ alloy shows a behavior quite typical for strong ferromagnets. In the ferromagnetic phase and in the vicinity of the Fermi level the total density of states is dominated by the Ni contribution, i.e., the Fermi level is situated in the minority subsystem on top of a peak coming from Ni, whereas in the majority channel this peak is almost fully occupied. This has the consequence that the entire average alloy moment will be localized on the Ni site while the Cu magnetic moment will be very small. Moreover, the subband resistivity in the spin-down direction will be larger than that in the other spin direction. Accordingly, the AMR is found to be positive on the basis of the two-current model (see also Secs. III C 2 and III B).

B. Magnetic properties

The generalized Slater-Pauling plots (GSP) for Ni$_x$Cr$_{1-x}$ and Ni$_x$Cu$_{1-x}$ alloy systems are given in Fig. 3. This generalization of the Slater-Pauling curves[26] permits us to include
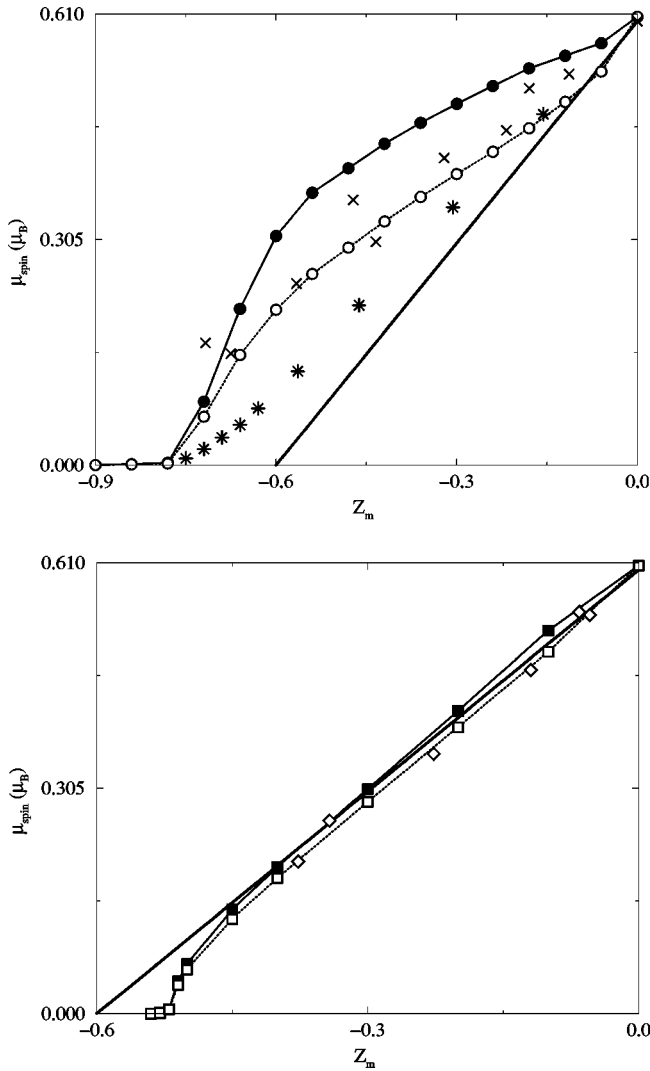
FIG. 3. Generalized Slater-Pauling plot for Ni_xCr_{1-x} (top) and Ni_xCu_{1-x} (bottom). The average alloy moments μ_{spin} (in μ_B units) calculated fully relativistically are represented by full symbols and the scalar-relativistic data are given by open symbols. Circles are used for Ni_xCr_{1-x} and squares for Ni_xCu_{1-x}. The experimental data were taken from Ref. 16 (*) and Ref. 26 (×) for Ni_xCr_{1-x}, and from Ref. 26 (◇) for Ni_xCu_{1-x}. The straight line with the 45° slope corresponds to $\mu_{spin}=Z_m+0.6$ as function of the average magnetic valence Z_m.

in the overview alloy systems like Ni_xCr_{1-x}, which show a pronounced departure from the regular behavior in a Slater-Pauling plot (SP). The plots are based on the magnetic valence Z_m that for a binary alloy system A_xB_{1-x} is defined as the concentration-weighted average:

$$Z_m = xZ_m^A + (1-x)Z_m^B, \tag{8}$$

$$Z_m^{A(B)} = 2N_d^{\uparrow;A(B)} - Z_v^{A(B)} \tag{9}$$

with $Z_v^{A(B)}$ the chemical valence and $N_d^{\uparrow;A(B)}$ the number of d electrons in the majority spin subsystem. This quantity immediately allows one to distinguish between strong and weak ferromagnets. A strong ferromagnet, e.g., would have either

$N_d^{\uparrow}=5$, i.e., fully occupied $d^{\uparrow}$ bands, or entirely empty $d^{\uparrow}$ bands and consequently $N_d^{\uparrow}=0$. Taking the chemical valence Z_v according to the periodic table, one gets $Z_m^{Ni}=0$, $Z_m^{Cr}=-6$, and $Z_m^{Cu}=-1$, respectively. This leads to the average alloy moment:

$$\mu_{spin} = Z_m + 2N_{sp}^{\uparrow}. \tag{10}$$

As it was shown in Ref. 37, the number of sp electrons in the majority spin subsystem $N_{sp}^{\uparrow}$ is a small noninteger, typical between 0.3 and 0.45. Although all the calculated spin moments for Ni_xCr_{1-x} lie between $\mu_{spin}=Z_m+0.9$ and $\mu_{spin}=Z_m+0.6$, in Fig. 3 only the latter straight line is given.

A first inspection of Fig. 3 shows that the average alloy moments calculated fully relativistically are always bigger than those obtained scalar-relativistically, but there is no qualitative change in the variation of μ_{spin} with Z_m. Some experimental data[16] for Ni_xCr_{1-x} show a stricter linearity than our calculated μ_{spin} or that listed in Ref. 26 (see Fig. 3 top). It is noteworthy that the latter experimental values for μ_{spin} show essentially the same variation with concentration as ours and that they are mostly situated between the fully relativistic and scalar-relativistic results. A better agreement between experiment and theory is obtained for Ni_xCu_{1-x} (Fig. 3 bottom), where the linearity of μ_{spin} versus Z_m is more pronounced than for Ni_xCr_{1-x}. Obviously, both alloy systems investigated here present a strong deviation from the linear behavior of $\mu_{spin}(Z_m)$ near the paramagnetic-ferromagnetic transition region. In the case of Ni_xCr_{1-x} this can be explained by the changes in the electronic structure near the critical concentration (see Sec. III A). In the case of Ni_xCu_{1-x} the main source of the deviation seems to be percolation, which assists the magnetic phase transition.[17]

The μ_{spin} curve of Ni_xCu_{1-x} outside the "transition region" (say $Z_m > -0.45$) is parallel to $Z_m + 0.6$. Hence, based on the definition given by Williams and co-workers,[37] we can conclude that Ni_xCu_{1-x} for $x>55$ at. % Ni is a strong ferromagnet. For $45.5 < x < 55$ at. % Ni the alloy system Ni_xCu_{1-x} turns out to be a weak ferromagnet because the average alloy moment lies below $Z_m + 0.6$ and $\mu_{spin}(Z_m)$ has a slope different from 45°.

As it was anticipated by Williams et al.,[26] the calculated average alloy moment of Ni_xCu_{1-x} follows closely the straight line $Z_m + 0.6$. If we were to identify $0.6\mu_B$ in the expression $\mu_{spin}=Z_m+0.6$ with the appropriate value of μ_{spin}^{Ni} instead of $2N_{sp}^{\uparrow}$, the average Ni_xCu_{1-x} moment could be written $\mu_{spin}=\mu_{spin}^{Ni}-x_{Cu}$ [see also Eq. (8) for $Z_m^{Ni}=0$ and $Z_m^{Cu}=-1$]. Remembering that $Z_v^{Cu}-Z_v^{Ni}=1$, Eq. (10) could then be replaced by Mott's formula[38]

$$\mu_{spin} = \mu_{spin}^{Ni} - x_{Cu}(Z_v^{Cu} - Z_v^{Ni}). \tag{11}$$

Although this formula was derived by Mott within the rigid-band model, it does not imply that this model yields good results for Ni_xCu_{1-x}. On the other hand, our SPR-KKR-CPA calculations show explicitly that Eq. (11) does not require the applicability of the rigid-band model. The reason for this is the basic assumption leading to Eq. (10): $N_{sp}^{\uparrow}$ and $N_d^{\uparrow}$ should remain unchanged upon alloying. In other words, Eq. (10) and consequently Eq. (11) are not dependent on the particular configuration of the bands or on the method used to calculate these.

Similar, if the average alloy moment of Ni$_x$Cr$_{1-x}$ followed the line $Z_m + 0.6$, Eq. (10) could be replaced by Friedel's formula[34]

$$\mu_{spin} = \mu_{spin}^{Ni} - x_{Cr}[10 + (Z_v^{Cr} - Z_v^{Ni})]. \qquad (12)$$

This expression can be seen as an extended Mott formula that accounts for the virtual bound states. Indeed, due to the bound state crossing the Fermi level, one expects to have five electrons less in the majority spin subsystem leading to five electrons more in the other spin channel. Thus one has to consider a change of ten electrons in Eq. (11). Although Eq. (12) gives the proper physics behind Eq. (10), Ni$_x$Cr$_{1-x}$ shows an appreciable deviation from the expected trend even when the generalized Slater-Pauling plot is used to analyze μ_{spin}. Moreover, Eq. (12) overestimates the critical concentration. Indeed, requiring just to have a positive average alloy moment for Ni$_x$Cr$_{1-x}$, Eq. (12) fixes the critical concentration above 90 at. % Ni in contrast to the observed or calculated value, which is around 85 at. % Ni.

All the features of $\mu_{spin}(Z_m)$ presented above for both alloy systems investigated here find a rather simple explanation if one closely inspects the total number of electrons in the majority spin subsystem ($N^{\uparrow} = N_{sp}^{\uparrow} + N_d^{\uparrow}$) versus the magnetic valence. In order to trace the differences in the calculated average alloy moment for Ni$_x$Cu$_{1-x}$ and Ni$_x$Cr$_{1-x}$, $N^{\uparrow}$ gives a better insight than $N_{sp}^{\uparrow}$ or $N_d^{\uparrow}$ alone. The reason for this is the charge transfer observed between the different spin subsystems and l channels, because this mechanism makes $N_{sp}^{\uparrow}$ to be around 0.70 electrons instead of the expected value of 0.30 and less than five electrons for $N_d^{\uparrow}$. These assumptions used for setting up the Slater-Pauling plots are obviously not consistent with our SPR-KKR-CPA results.

Finally, it should be emphasized that the average alloy moment of Ni$_x$Cu$_{1-x}$ is primarily provided by the magnetic moments localized on Ni sites. The Cu moments are very small (few $10^{-3} \mu_B$). In contrast, Cr possesses an appreciable local moment in the concentration range, where Ni$_x$Cr$_{1-x}$ is magnetically ordered and is always aligned antiparallel to the local magnetic moments of Ni.

C. Transport properties

1. Isotropic residual resistivity

The results of the CPA-based calculations of the isotropic residual resistivity are shown and compared to experimental data in Fig. 4. Obviously, the overall concentration dependence of the isotropic residual resistivity ($\bar{\rho}$) determined experimentally is reproduced quite well. The reason for the remaining quantitative discrepancy between calculated and measured $\bar{\rho}$ is twofold. First, the theoretical residual resistivity is caused exclusively by chemical disorder in the approach used. Experimental data, however, always contain contributions coming from impurities, lattices defects, grain boundaries, phonons, magnons, etc.[20] Moreover, anomalies in the temperature dependence of the resistivity can introduce further complications when the data are extrapolated to 0 K. This applies to both alloy systems investigated here.[21,39]
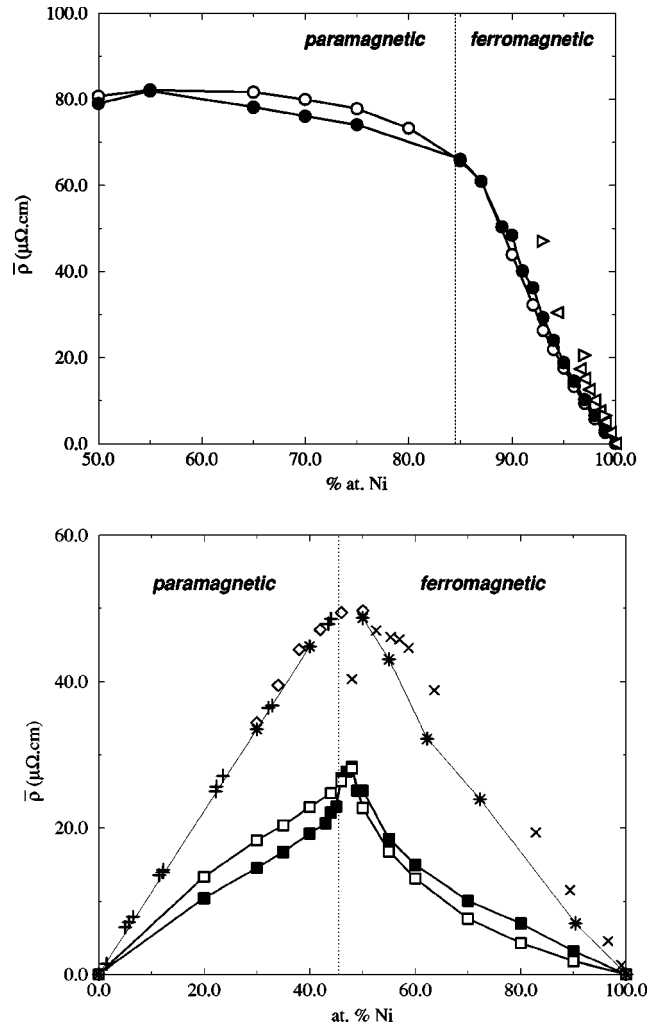
FIG. 4. Isotropic residual resistivity vs Ni concentration for Ni$_x$Cr$_{1-x}$ (top) and Ni$_x$Cu$_{1-x}$ (bottom). Full symbols denote results obtained in fully relativistic calculations, while open symbols resulted from the two-current model calculations within a scalar-relativistic scheme. Circles are used in case of Ni$_x$Cr$_{1-x}$ and squares for Ni$_x$Cu$_{1-x}$. The vertical dotted line indicates the critical concentration obtained theoretically. Experimental values were taken for Ni$_x$Cr$_{1-x}$ from Refs. 48 ($\triangleleft$), 49 ($\triangleright$) and for Ni$_x$Cu$_{1-x}$ from Refs. 19 ($\times$), 20 ($\diamond$), 39 ($+$), and 50 ($*$).

One should note that transport calculations of the kind presented here mostly underestimate the resistivity due to these reasons.

For Ni$_x$Cu$_{1-x}$ the difference between experimental and calculated $\bar{\rho}$ takes its maximum near the critical composition, where the paramagnetic-to-ferromagnetic phase transition occurs (Fig. 4, top panel). One reason for this could be the clustering effects known in the transition region,[40] which cannot be incorporated in a plain CPA-based resistivity calculation.[41] The clusters built up mainly by Ni atoms appear at concentrations above 44 at. % Ni (Ref. 20) and persist up to 50 at. % Ni (Ref. 42). Due to their highly localized magnetic properties, these spin clusters are responsible for anomalies in the temperature[19,20] and concentration dependence[17] of the resistivity. Their impact on the magnetic

behavior of Ni_xCu_{1-x} in the transition region is even more pronounced. The initial paramagnetic, Cu-rich alloy turns into a superparamagnetic regime containing magnetic clusters with up to $10\mu_B$ moments with increasing Ni content[22,43] such that the onset of ferromagnetism is preceded by a spin-glass-like ordering.[23,24]

In spite of the limitations of the CPA due to its single-site character (averaging out the effect of neighbors around the scattering centers), it nevertheless allows us to reproduce the critical concentration with an accuracy of 1 at. % Ni. Based on our calculated average alloy magnetic moments and AMR ratios we found 45.5 at. % Ni, while the measurements[17] show the appearance of ferromagnetism at 44.5 at. % Ni. Furthermore, the maximum of $\bar{\rho}$ is positioned in very good agreement with experimental data. Probably due to the existence of magnetic clusters $\bar{\rho}$ does not achieve its maximum at the critical concentration as it was believed in the past.[44] Hence the different curvature of $\bar{\rho}(x)$ on both sides of the maximum is related rather to the subband resistivities and to the density of states at the Fermi level, $n(E_F)$ (see Sec. III A) than to the magnetic order in Ni_xCu_{1-x}.

Comparing the subband resistivities $\rho^\uparrow$ and $\rho^\downarrow$ as a function of Ni concentration obtained from scalar-relativistic spin polarized KKR-CPA calculations (not presented here), one observes that $\bar{\rho}$ closely follows the concentration dependence of $\rho^\uparrow$. This is a direct consequence of Eq. (7) and of the fact that $\rho^\downarrow$ is more than twice as large as $\rho^\uparrow$ almost over the entire concentration range of ferromagnetic Ni_xCu_{1-x}.

Comparison of the fully relativistic isotropic resistivity $\bar{\rho}$ with that calculated using the two-current model (hence the scalar-relativistic scheme) reveals that the inclusion of the spin-orbit coupling reduces the difference between the theoretical and experimental data for the ferromagnetic phase. In contrast, SOC has the opposite effect on the paramagnetic $\bar{\rho}$ and lowers the residual resistivity, thus improving agreement with the experiments.

The same impact of SOC on $\bar{\rho}$ can be observed in the case of Ni_xCr_{1-x}—compare the fully relativistic data with those obtained scalar-relativistically in Fig. 4 (top). SOC lowers the residual resistivity in the paramagnetic phase and increases it in the ferromagnetic regime. Unfortunately, no experimental data are available below 90 at. % Ni in the case of Ni_xCr_{1-x} and hence the comparison of our results with the experimental data cannot be made for the whole range of concentrations. The lack of experimental transport data for Ni_xCr_{1-x} can be explained to some extent by the primary interest in the effect of scattering centers in Ni, which needs to be studied only for dilute alloys. In the Ni-rich region, where experimental $\bar{\rho}$ data are available, our calculated data are found to be always lower (several possible sources for the deviation were given above) than those measured and show an appreciable departure from a linear variation. This is understandable because $\bar{\rho}$ is proportional to the impurity concentration only as long as the alloy systems are dilute.

In contrast to Ni_xCu_{1-x}, the residual resistivity $\bar{\rho}$ for Ni_xCr_{1-x} closely follows the subband resistivity $\rho^\downarrow$ as long as the alloy system is ferromagnetic, namely for Ni concen-
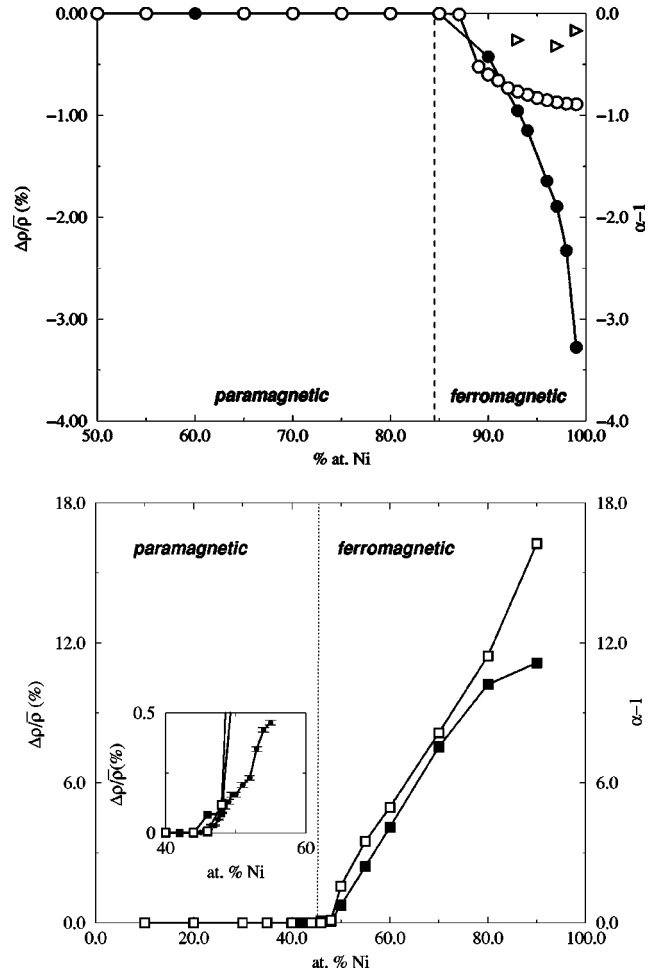
FIG. 5. Anomalous magnetoresistance (AMR) as a function of Ni concentration for Ni_xCr_{1-x} (top) and Ni_xCu_{1-x} (bottom), respectively. Full symbols give the AMR ratio $\Delta\rho/\bar{\rho}$ obtained based on the SPR-KKR-CPA method and open symbols are used for $\alpha-1$, where $\alpha=\rho^\downarrow/\rho^\uparrow$ is the ratio of subband resistivities $\rho^\uparrow,\rho^\downarrow$ calculated within the framework of scalar-relativistic SP-KKR-CPA, circles are used in case of Ni_xCr_{1-x} and squares for Ni_xCu_{1-x}, and triangles ($\triangleright$) stand for the experimental AMR values of Ni_xCr_{1-x} (Ref. 49). The inset in the bottom panel contains the experimental AMR ratios for Ni_xCu_{1-x} ($\bullet$) together with the error bars as given in Ref. 17.

trations above the critical concentration 84.5 at. % Ni. As expected from the density of states (see Sec. III A, Fig. 1) that exhibits a higher value at the Fermi level in the majority subsystem than in the minority one due to the VBS induced by Cr, $\rho^\uparrow$ is twice as large as $\rho^\downarrow$.

2. Anomalous magnetoresistance ratio

The fully relativistic results for the AMR ratio of Ni_xCr_{1-x} and Ni_xCu_{1-x} are given in Fig. 5. For Ni_xCr_{1-x} the calculations predict a strong negative AMR ratio in the ferromagnetic regime. Experimental values are also negative, but their absolute values are much smaller. It is quite probable that impurities present in the samples weakened the influence of Cr, which is due to its VBS. This influence can

easily be diminished when impurities are added, which affect the density of states in a different way.

For Ni_xCu_{1-x} the AMR ratio rises from 0% to about 11% as one goes from the onset of ferromagnetism at 45% Ni to pure nickel. Experimental work shows a very similar behavior, except that the AMR ratio in Ni-rich alloys is only abound 6%.[4] A similar discrepancy was found in the alloy system Ni_xFe_{1-x} and was explained by a higher experimental residual resistivity caused by an influence not included in the calculations, such as impurities, lattice defects, or thermal scattering.[10] This additional contribution naturally reduces the AMR ratio as is evident from the definition in Eq. (2). As the experimental residual resistivity of Ni_xCu_{1-x} is about twice the calculated one, this explication seems very plausible.

The concentration dependence of $\alpha - 1$, α is the ratio of subband resistivities $\rho^\downarrow / \rho^\uparrow$, is also displayed in Fig. 5. According to Eq. (6) these two quantities are not identical, but connected via γ, which is a factor thought to be related to the strength of the SOC.[33] However, its concentration dependence is unknown and it is often assumed to be a constant with a value of about 0.01 in the case of Ni-based alloys.[15] This value of γ yields AMR ratios in a satisfactory agreement with the experimental data in dilute alloys. However, for concentrated alloys γ is not constant (not even in the Ni-rich part; see Fig. 5). One possibility for obtaining γ is to compare the fully relativistically calculated AMR ratio with $\alpha - 1$. This way, γ was indeed found to be strongly concentration dependent in the case of Co_xPd_{1-x} and Co_xPt_{1-x}.[9] Proceeding in a similar manner here, i.e., scaling $\alpha - 1$ to fit the fully relativistic $\Delta\rho / \bar{\rho}$ (plots not shown here), it turns out that γ varies quadratically with the Ni content, having a minimum around 93 at. % Ni in the case of Ni_xCr_{1-x} and with a maximum at 72 at. % Ni for Ni_xCu_{1-x}.

For Ni_xCr_{1-x} alloys both the fully relativistic AMR ratio and $\alpha - 1$ calculated scalar-relativistically are negative as long as the ferromagnetic order persists. This is quite easy to understand in terms of the two-current model, i.e., on the basis of Eq. (6). Because the Cr-induced VBS at the Fermi level makes $\rho^\uparrow$ larger than $\rho^\downarrow$ for Ni content above the critical concentration (84.5 at. % Ni), it follows that $\alpha = \rho^\downarrow / \rho^\uparrow < 1$.

As it was demonstrated by the AMR measurements of Stampe and Williams,[17] the magnetic phase transition in Ni_xCu_{1-x} is strongly influenced by percolation. As one can see in the inset of Fig. 5 (bottom), our CPA-based calculations cannot follow closely this process, although some of the calculated AMR ratio values agree well with those measured. The reason for this is that the CPA calculations can follow the fractional power concentration dependence of the spin magnetic moment as predicted by percolation theory[45] only in the nearest vicinity of the critical concentration (although the third-power dependence of the AMR ratio on the spin magnetic moment predicted by the localized magnetic model[46,47] is reproduced in a very satisfactory manner by our CPA calculations). In conclusion, the variation of the AMR as a function of Ni content in the transition region (i.e., between 43 and 50 at. % Ni) is caused by the spin-orbit coupling arising from the orbital component of the total magnetic moment localized on the scattering sites.

IV. SUMMARY

The electronic, magnetic, and galvanomagnetic properties of the fcc alloy systems Ni_xCr_{1-x} and Ni_xCu_{1-x} were investigated in two different ways: by treating the alloy fully and scalar-relativistically. CPA-based calculations provide the critical concentrations at which the paramagnetic-to-ferromagnetic phase transition takes place with an accuracy of 1 at. % Ni for both alloy systems. Furthermore, the residual resistivity and AMR ratio is obtained in satisfying agreement with measurements. The different sign of the AMR ratio for the two alloys is correctly reproduced by the calculations. Although the two-current model seems to work better than the fully relativistic scheme in the paramagnetic phase, the ferromagnetic phase definitively requires a fully relativistic treatment. However, the AMR for Ni_xCu_{1-x} calculated using the CPA shows a significant departure with respect to the measured values, because the phase transition is strongly influenced by percolation. For high Ni contents, on the other hand, the dependence of the AMR on the Ni concentration is reproduced.

For Ni_xCr_{1-x} we showed that the relatively sharp peak in the density of states near the Fermi level comes from Cr and exists in the ferromagnetic as well as paramagnetic phase. The investigation of the magnetic properties of Ni_xCr_{1-x} and Ni_xCu_{1-x} have shown that the departure of the calculated average magnetic alloy moment from the expected general trend can be substantially reduced using the generalized Slater-Pauling plot.

[1] D.A. Thompson, L.T. Romankiw, and A.F. Mayadas, IEEE Trans. Magn. **11**, 1039 (1975).

[2] M.N. Baibich, J.M. Broto, A. Fert, F.N. Van Dau, and F. Petroff, Phys. Rev. Lett. **61**, 2472 (1988).

[3] A.P. Ramirez, J. Phys.: Condens. Matter **9**, 8171 (1997).

[4] J. Smit, Physica (Amsterdam) **16**, 612 (1951).

[5] J. Banhart and H. Ebert, Europhys. Lett. **32**, 517 (1995).

[6] R. Kubo, J. Phys. Soc. Jpn. **12**, 570 (1957).

[7] D.A. Greenwood, Proc. Phys. Soc. London **71**, 585 (1958).

[8] J. Banhart, A. Vernes, and H. Ebert, Solid State Commun. **98**, 129

(1996).

[9] H. Ebert, A. Vernes, and J. Banhart, Phys. Rev. B **54**, 8479 (1996).

[10] J. Banhart, H. Ebert, and A. Vernes, Phys. Rev. B **56**, 10 165 (1997).

[11] H. Ebert, A. Vernes, and J. Banhart, Solid State Commun. **104**, 243 (1997).

[12] H. Ebert, A. Vernes, and J. Banhart, Solid State Commun. **113**, 103 (1999).

[13] H. Ebert, H. Freyer, A. Vernes, and G.-Y. Guo, Phys. Rev. B **53**, 7721 (1996).

[14] H. Ebert, H. Freyer, and M. Deng, Phys. Rev. B **56**, 9454 (1997).

[15] O. Jaoul, I.A. Campbell, and A. Fert, J. Magn. Magn. Mater. **5**, 23 (1977).

[16] M.J. Besnus, Y. Gottehrer, and G. Munschy, Phys. Status Solidi B **49**, 597 (1972).

[17] P.A. Stampe and G. Williams, J. Phys.: Condens. Matter **9**, 9251 (1997).

[18] A. Amamou, F. Gautier, and B. Loegel, J. Phys. F: Met. Phys. **5**, 1342 (1975).

[19] J. Crangle and P.J.L. Butcher, Phys. Lett. A **32A**, 80 (1970).

[20] R.W. Houghton, M.P. Sarachik, and J.S. Kouvel, Phys. Rev. Lett. **25**, 238 (1970).

[21] T.F. Smith, R.J. Tainsh, R.N. Shelton, and W.E. Gardner, J. Phys. F **5**, L96 (1975).

[22] H. Claus, Phys. Lett. **51A**, 283 (1975).

[23] C.J. Tranchita and H. Claus, Solid State Commun. **27**, 583 (1978).

[24] D.W. Carnegie, Jr., C.J. Tranchita, and H. Claus, J. Appl. Phys. **50**, 7318 (1979).

[25] F.C. Schwerer and J. Silcox, Phys. Rev. B **1**, 2391 (1970).

[26] A.R. Williams, V.L. Moruzzi, A.P. Malozemoff, and K. Terakura, IEEE Trans. Magn. **MAG-19**, 1983 (1983).

[27] J.S. Faulkner and G.M. Stocks, Phys. Rev. B **21**, 3222 (1980).

[28] P. Weinberger, *Electron Scattering Theory for Ordered and Disordered Matter* (Oxford University Press, Oxford, 1990).

[29] W.H. Butler, Phys. Rev. B **31**, 3260 (1985).

[30] J.C. Swihart *et al.*, Phys. Rev. Lett. **57**, 1181 (1986).

[31] H. Ebert, B. Drittler, and H. Akai, J. Magn. Magn. Mater. **104-107**, 733 (1992).

[32] J.W.F. Dorleijn, Philips Res. Rep. **31**, 287 (1976).

[33] I.A. Campbell, A. Fert, and O. Jaoul, J. Phys. C **3**, S95 (1970).

[34] J. Friedel, Nuovo Cimento, Suppl. **7**, 287 (1958).

[35] J. Kanamori, J. Appl. Phys. **36**, 929 (1965).

[36] N. Stefanou, A. Oswald, R. Zeller, and P.H. Dederichs, Phys. Rev. B **35**, 6911 (1987).

[37] A.P. Malozemoff, A.R. Williams, and V.L. Moruzzi, Phys. Rev. B **29**, 1620 (1984).

[38] N.F. Mott and H. Jones, *The Theory of the Properties of Metals and Alloys* (Clarendon Press, Oxford, 1936).

[39] S. Legvold, D.T. Peterson, P. Burgardt, R.J. Hofer, B. Lundell, T.A. Vyrostek, and H. Gartner, Phys. Rev. B **9**, 2386 (1974).

[40] D.H. Seib and W.E. Spicer, Phys. Rev. B **1**, 937 (1970).

[41] P.L. Rossiter, J. Phys. F **11**, 2105 (1981).

[42] A. Kidron, Phys. Rev. B **1**, 939 (1970).

[43] J.S. Kouvel and J.B. Comly, Phys. Rev. Lett. **24**, 598 (1970).

[44] J.C. Ododo and B.R. Coles, J. Phys. F **7**, 2393 (1977).

[45] J.W. Essam, Rep. Prog. Phys. **43**, 53 (1980).

[46] M.S.S. Brooks and T. Egami, J. Phys. C **6**, 513 (1973).

[47] M.S.S. Brooks and T. Egami, J. Phys. C **6**, 3719 (1973).

[48] F.C. Schwerer and J.W. Conroy, J. Phys. F **1**, 877 (1971).

[49] P. Muth and W. Heimke, Phys. Status Solidi A **126**, K69 (1991).

[50] H.M. Ahmad and D. Greig, J. Phys. (Paris), Colloq. **35**, C4 (1974).